Express Polymer Letters Vol.18, No.2 (2024) 118–132
Available online at www.expresspolymlett.com
https://doi.org/10.3144/expresspolymlett.2024.10

Research article

Evaluating the influence of chemical composition and morphology of waxes on the fusion behaviour of rigid PVC

Johannes Lodewiekus Barnard[1], *Divann Dale Robertson*[1,2*], *Albert Johannes van Reenen*[1]

[1]Department of Chemistry and Polymer Science, University of Stellenbosch, Private Bag X1, 7602, Matieland, South Africa
[2]Contextualize (Pty) Ltd, Wavecrest, 7140 Strand, South Africa

Received 31 August 2023; accepted in revised form 25 October 2023

Abstract. A set of linear Fischer-Tropsch (FT) waxes were oxidized to various degrees by utilizing an ozonolysis method. These waxes were comprehensively characterized in terms of their chemical composition, thermal behaviour, molecular weight distributions, and overall polarity using various analytical techniques, including Fourier transform infrared spectroscopy (FTIR), nuclear magnetic resonance spectroscopy (NMR), differential scanning calorimetry (DSC), high temperature size exclusion chromatography (HT-SEC) along with normal and reverse-phase high temperature solvent gradient interaction chromatography (HT-SGIC). Application-based studies were performed by evaluating the behaviour of these waxes in unplasticized polyvinyl chloride (uPVC) formulations. Analyses included hot melt mixing, single screw extrusion, scanning electron microscopy coupled with energy dispersive X-ray spectroscopy (SEM-EDS), and torque rheometry. Through a combination of these techniques, the lubrication mechanism of these waxes could be explained by the Rabinovitch model. It was found that a combination of molecular size and degree of polarity play a vital role in the migration of the waxes and therefore ultimately impacts the fusion behaviour of the overall polyvinyl chloride (PVC) formulation. Results indicate that fusion times can greatly be altered when using oxidised waxes, and this could be promising for the development of multifunctional lubricant systems.

Keywords: *additive, toughness, PVC, fusion, wax*

1. Introduction

Second to polyolefins, polyvinyl chloride (PVC) is one of the most used polymers in the industry [1–6]. PVC owes its popularity to its many desirable properties, such as low cost, high strength, electrical resistivity, as well as flame retardant properties. Flexible PVC is produced by incorporating a plasticizer, whereas unplasticized PVC (uPVC) is produced in the absence of a plasticizer and is also known as rigid PVC. Flexible PVC is used in textiles, electrical insulation, or medical apparatus, and rigid PVC is extruded into profiles for use in piping or door and window profiles [7, 8]. The process of extrusion is, however, very challenging as PVC readily degrades at high processing temperatures [9]. During the processing of most commodity plastics, the addition of wax lubricants as processing aids and viscosity modifiers is of great importance to the industry [10]. Similarly, to obtain sufficient PVC fusion, various lubricants are incorporated during its extrusion process. Several studies have shown that enhancing the fusion level leads to an improvement in mechanical properties, either resulting in a plateau or, in the case of impact strength and related characteristics, reaching a maximum value [11]. For uPVC, lubrication is one of the three most important parameters to achieve the desired extrusion products, together with the instrumentation and the PVC resin [12]. The current model

---

[*] Corresponding author, e-mail: ddr@sun.ac.za

used to describe PVC lubrication was proposed by Rabinovitch and coworkers [12, 14] and [13, 15], which is based on classifying lubricants as either surfactants or slip agents. This model is based on the interaction between a surfactant and a slip agent and how they interact with the surrounding metal interface of an extruder and the PVC resin particles. A metal salt such as calcium stearate (CaSt) is used as a surfactant, and a hydrocarbon molecule such as paraffin wax is used as a slip agent. The model was proposed after conducting various tests and stating that polar moieties would associate within polar regions and that nonpolar moieties would associate with areas of a nonpolar nature. These polar areas would, therefore, be the polar PVC resin and the slightly oxidized polar metal interface, which leaves the only nonpolar region in the system to be the nonpolar wax and the stearate tail of CaSt.

Functional waxes such as amide or oxidized waxes are gaining popularity as they could provide the function of both surfactant and slip agent. Authors such as Treffler [16] have shown that species such as montanic acid ester waxes and fatty acid amides show promise as both internal and external lubricant or surfactant and slip agent type behaviour. Exactly how they would fit into Rabinovitch's model is, however, unknown [5].

This study aims to build on a previous study by the research group wherein it was shown that internal lubrication promotes external lubricant dispersion and that there exists a competition effect between oxidized waxes and internal lubricants [17]. In this current study, an approach was taken to synthesize and fully characterize oxidized waxes in terms of their thermal behaviour, chemical, and morphological compositions, using a vast array of analytical tools. These waxes were incorporated in PVC blends and evaluated with torque rheometry to understand the wax contributions to the performance of the resultant PVC formulations.

2. Materials

Commercially available suspension-grade PVC resin was sourced from Sasol SA (S6721, *K*-value = 67, South Africa). Calcium stearate (CaSt) was obtained from Dover Chemical Corporation (Doverlube CA-21, particle size = minimum 95% <75 µm, Ohio, USA). Two hydrocarbon Fischer-Tropsch (FT) waxes with varying molecular chain lengths were supplied by Juniper SP LLC (J75 and J100, Houston, USA), and a tin-based heat stabilizer was sourced from PMC Organometallix Inc. (Thermolite 176, USA). In the melt-mixing and screw freezing experiments, higher concentrations of wax and CaSt were used to ensure their detection during scanning electron microscopy (SEM) analyses. During fusion testing, commercially relevant lubricant concentrations were used to formulate PVC blends that are comparable to that of industry standards. Formulation ingredients were in alignment with acceptable limits as documented within the TR-2 guidelines published by the Plastics Pipe Institute (PPI). Table 1 lists the concentrations for the various compounds during the respective experimental protocols.

Table 1. Formulation composition for various experimental protocols.

Experimental protocol	**Concentration [phr]**			
	PVC	**CaSt**[1]	**Wax**	**Stabilizer**
Melt mixing	100	5	5	1
Screw freezing	100	5	5	1
Fusion testing	100	0.6	0.9	0.6

[1] The concentration of calcium stearate was reduced to zero for binary blends.

3. Experimental

3.1. Oxidation of waxes

Two linear FT waxes, J75 and J100, were chosen for this investigation. These two waxes were obtained from the same Fischer-Tropsch synthesis (FTS) master batch. They were respectively obtained through controlled distillation. J100 is a higher melting wax with melting temperature (T_m) ≈ 100 °C, and J75 is a medium melting wax (T_m ≈ 75 °C). In this experiment, both these neat waxes were subjected to ozonolysis, which resulted in two sets of waxes with varying degrees of oxidation (see Table 2). Ozonolysis was carried out by bubbling ozone (O_3) gas through the molten wax solution under constant stirring. Ozone gas was produced by controlled feeding of oxygen (O_2) gas into an A2Z electric discharge ozoniser (Fisher Scientific, Meckenheim, Germany). Ozone was introduced at a rate of 6 g/h and was monitored by keeping the O_2 flow (50 l/h) and electrical current (1 A) constant. J75 and J100 were heated to 120 and 140 °C, respectively, to ensure that the waxes remained in the molten state throughout the oxidation process. The degree of oxidation was monitored offline using attenuated total reflectance Fourier transform infrared (ATR-FTIR) spectroscopy.

3.2. Fourier transform infrared spectroscopy (FTIR)

Analyses were conducted on a Thermo Scientific Nicolet iS10 FTIR (Thermo Fisher Scientific, Waltham, USA) spectrometer equipped with a diamond crystal. Scans were performed at a resolution of 4 cm^{-1}, and 64 scans were taken. OMNIC (version 9, Thermo Fisher Scientific, South Africa) processing software was used for data analysis.

3.3. Quantitative ^{13}C nuclear magnetic resonance spectroscopy (^{13}C-NMR)

^{13}C-nuclear magnetic resonance (^{13}C-NMR) spectra were acquired on a Varian Unity INOVA 600 MHz (Varian Inc. USA, supplied by SMM South Africa) liquid state NMR spectrometer at 120 °C. All samples (70–75 mg) were dissolved in 0.6 ml deuterated 1,1,2,2,-tetrachloroethane (d_2-TCE) (purity $\geq$ 99.5%, Sigma Aldrich, South Africa). A 90° pulse angle with an acquisition time of 0.87 s and a relaxation delay of 15 s was used. The average number of scans was 4000. Chemical shifts were referenced to the backbone methylene (CH_2) peak at 30 ppm, and spectra were analysed with Mnova software.

3.4. Differential scanning calorimetry (DSC)

Endothermic melting and exothermic crystallization behaviour of the samples were analysed using a TA instruments Q100 (Delaware, USA) differential scanning calorimeter, calibrated with indium metal according to standard procedures. A three-step cycle was implemented wherein each sample (≈4 mg) was heated from 25 to 200 °C in the first cycle at a heating rate of 10 °C/min. This was done to remove any thermal history of the samples. Samples were kept isothermally at 200 °C for 3 min, after which they were cooled to 25 °C at 10 °C/min. During the ultimate step, the temperature was kept isothermally at 25 °C for 3 min and then heated to 200 °C. Data obtained from the second heating cycle was used for enthalpy calculations. The DSC measurements were conducted in an inert nitrogen atmosphere at a purge gas flow rate of 20 ml/min. Data was analysed using TA Universal Analysis software.

3.5. High temperature – size exclusion chromatography (HT-SEC)

Determination of the molecular weights and molecular weight distributions was carried out on a PL220 high temperature chromatography system (Polymer Laboratories, Church Stretton, UK) coupled to a differential refractive index (*RI*) detector. Polyethylene standards were used for calibration. Samples (≈4 mg) were dissolved in 1,2,4-trichlorobenzene (TCB) containing 0.025% butyl-hydroxytoluene (BHT) stabilizer (Sigma Aldrich, South Africa). The mobile phase had a flow rate of 1 ml/min, and the stationary phase consisted of three 300×7.5 mm PLgel Olexis columns (Agilent Technologies, UK) together with a 50×7.5 mm PLgel Olexis guard column. Sample volumes of 200 µl were injected at 160 °C.

3.6. High temperature - solvent gradient interaction chromatography (HT-SGIC)

Experiments were performed on a high temperature liquid chromatography system (PolymerChAR, Valencia, Spain), utilizing a solvent gradient during analyses. For solvent gradient elution, a high-pressure binary gradient pump (Agilent, Germany) was used. An evaporative light scattering detector (ELSD, model PL-ELS 1000, Agilent Technologies, UK) was used for all detection purposes.

3.7. Reverse-phase HT-SGIC

To separate the waxes according to their degree of nonpolar segments, a Hypercarb column (Hypercarb®, Thermo Scientific, Germany) with an internal diameter of 100×4.6 mm and packed with porous graphite particles having a particle diameter of 5 mm (making a surface area of 120 m^2/g) and pore size of 250 Å, was used. These separations occurred according to ethylene sequence length. The column was placed in an oven at 120 °C, and the mobile phase consisted of a solvent combination of decane and ortho-dichlorobenzene (o-DCB) (Sigma Aldrich, South Africa) with a constant flow rate of 0.5 ml/min. A sample concentration of 2 mg/ml was used, and 50 ml of each sample was injected for all the experiments. The evaporative light scattering detector (ELSD) settings used were as follow: a gas flow rate of 0.5 SLM, 140 °C nebulizer temperature, and an evaporative temperature of 200 °C.

3.8. Normal-phase HT-SGIC

In order to separate according to the polar segments of the waxes, a silica column (Nucleosil, Macherey-Nagel, Germany) with a 300×4.6 mm length and internal diameter packed with silica particles of 5 µm and a pore size of 300 Å, was used. The mobile phase flow rate was 0.5 ml/min. Samples were dissolved in decane prior to injection. 1-hexanol was used as desorption promoting solvent, and the flow rate was adjusted as needed. The ELSD settings were similar to that used for the reverse-phase HT-SGIC. Sample concentrations of 2 mg/ml were used, and 50 µl of each sample was injected.

3.9. Melt mixing

Hot-melt mixing was done by overhead stirring with a Heidolph mixer (Heidolph Instruments, RZR series, Schwabach, Germany), (2100 rpm) at 165 °C for 15 min. This temperature was chosen to ensure all the lubricants were above their melting temperatures. PVC blends were allowed to cool to room temperature before further analyses.

3.10. Extrusion and screw freezing

Extrusion was done on a Brabender Plasticorder PLE 651 extruder (Brabender, Duisburg, Germany) with a single screw barrel attachment ($L/D = 26.5:1$). The barrel was preheated at three zones. Zone one (feeding zone) was heated to 145 °C. Zone two (compression zone) was heated to 155 °C and zone three (metering zone) was heated to 190 °C. After some samples exited the die and effective extrusion had been established, the screw rotation was stopped for evaluation of the sample inside the barrel. Due to the poor heat stability of PVC and the risk of hydrochloric acid build-up, the screw was removed from the barrel while the heating elements were still active, using a hydraulic press. After the removal of the screw, the sample was allowed to cool down to room temperature. PVC material within the screw flights were sampled and submitted for microscopy analyses.

3.11. Scanning electron microscopy (SEM)

A Zeiss EVO MA15 (Carl Zeiss Microscopy, Jena, Germany) high resolution scanning electron microscope was used for imaging. Samples were mounted on aluminium stubs with double sided carbon tape and were coated with a thin (~10 nm) layer of gold, using an Edwards S150A gold sputter coater (Leica Microsystems, Wetzlar, Germany). A Zeiss 5-diode back scattered electron (BSE) detector (Zeiss NTS BSD) and Zeiss Smart SEM software were used to generate BSE images. Energy dispersive X-ray spectrometry (EDS) was performed using an Oxford Instruments® X-Max 20 mm^2 detector and Oxford Aztec software to analyze compositional distributions of the PVC blends. Beam conditions during the quantitative analysis and backscattered electron image analysis on the Zeiss EVO were 20 kV accelerating voltage, 8 nA probe current, with a working distance of 8.5 mm, and a beam current of 5 nA. The counting time was 10 s live-time.

3.12. Fusion testing

Fusion studies were performed on a Thermo Scientific torque rheometer (Haake Polylab OS, Thermo Ficher Scientific, Karlsruhe, Germany). The system was coupled to a Haake Rheomix OS lab mixer fitted with roller rotors. PVC blends were introduced to a preheated rheometer chamber, and two time-dependant torque measurements were conducted using a screw rotation speed of 65 rpm and experimental temperatures of 185 and 190 °C, respectively. The mass of each PVC blend was 65 g. Analyses were performed until a clear onset of degradation was observed. The general interpretation of a PVC fusion curve is shown in Figure 1, where an increased torque at point A represents the fusion event and region B represents the stable time of a formulation. From point A, the fusion time and torque can be obtained.

4. Results and discussion

4.1. Wax characterization

4.1.1. Fourier transform infrared spectroscopy (FTIR)

All infrared spectroscopy measurements were done off-line and a commercially available oxidized wax, namely Ceranox 40L90 (Sarpri, South Africa), with an acid number of 40 mg KOH/ml was used as a reference to track the degree of oxidation of the experimental waxes during ozonolysis. The relative intensity of the carbonyl band of the commercial wax was roughly 40% of the backbone methylene stretching vibrational band. These relative FTIR intensities

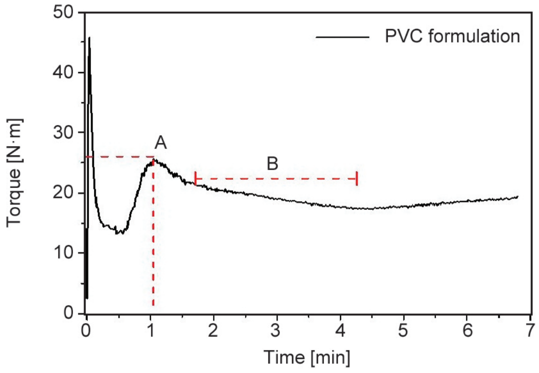

Figure 1. General illustration of a PVC fusion curve.

were used as an indication of the oxidation levels of the experimental waxes. FTIR spectra of the higher oxidized J75 wax and that of Ceranox 40L90 were in good agreement, especially in the carbonyl region, indicating similar degrees of oxidation. Thus, the sample was denoted as oJ75_40 to indicate the degree of oxidation to be roughly 40%. Two levels of oxidation were targeted, namely, 10 and 40%. Sample oJ75_40, however, did not exhibit a significant hydroxyl absorbance (Figure 2a). Figure 2b shows the expanded carbonyl absorbance range. Multiple carbonyl band splitting could be observed, possibly contributed by different carbonyl species. The main carbonyl band at 1716 cm^{-1} had the same relative intensity for both waxes. Additional shoulders in the carbonyl range were observed at 1734 and 1776 cm^{-1}, respectively. For both these signals, sample oJ75_40 exhibited a slightly lower signal intensity compared to the Ceranox 40L90 sample, indicating that resultant oxygenated species may differ depending on the method of oxidation and suggesting that care should be taken when classifying and comparing oxidized waxes solely on acid numbers. It was, however, unknown which commercial method was used during the synthesis of Ceranox 40L90. Ozonolysis of J100 yielded similar results, which are also shown in Figure 2. Figure 2b shows the progression of oxidation for J75 and J100. In both cases, the carbonyl bands increased with oxidation time. Both samples that were highly oxidized showed a new band at 1167 cm^{-1} associated with C–O stretching [18]. Hereafter, it was decided to conduct further investigation into the type of oxygen moieties that were developing during the ozonolysis reactions.

Table 2. Oxidized waxes from ozonolysis protocol.

FT wax	Code	O_3[1] [wt%]	Oxidation[2] [mol%]
J75	oJ75_10	24	10
	oJ75_40	92	40
J100	oJ100_10	15	10
	oJ100_40	90	40

[1] Percentages were calculated as amount of ozone [g]/total amount of wax [g].

[2] Percentages were calculated as maximum carbonyl absorbance (1715 cm^{-1})/maximum methylene absorbance (2920 cm^{-1}).

4.1.2. Quantitative ^{13}C nuclear magnetic resonance spectroscopy (^{13}C-NMR)

As it was quite clear that there were differences between the FTIR spectra of the waxes modified by the ozonolysis treatment and the commercially available oxidized wax, further investigation into the chemical composition of the waxes was conducted using quantitative ^{13}C nuclear magnetic resonance (^{13}C-NMR) spectroscopy. From Figures 3 and 4, the upfield chemical shift region of samples J75 and J100 can be seen, respectively. The saturated chain end carbons (1s, 2s, 3s, and 4s) can be seen at 14.2, 22.9, 32.2, and 29.6 ppm, respectively, as well as the backbone methylene (CH_2) carbons at 30 ppm. All spectra were normalized to the backbone methylene signals. The chain end carbons had greater intensities for the J75 waxes compared to the J100 waxes. This is shown in Table 3, where the J75 chain end carbons showed signal integration values of ±10 mol%, compared to sample J100, which showed signals of ±5.0 mol%. This was due to the higher relative concentration of chain end carbons to the backbone carbons for the

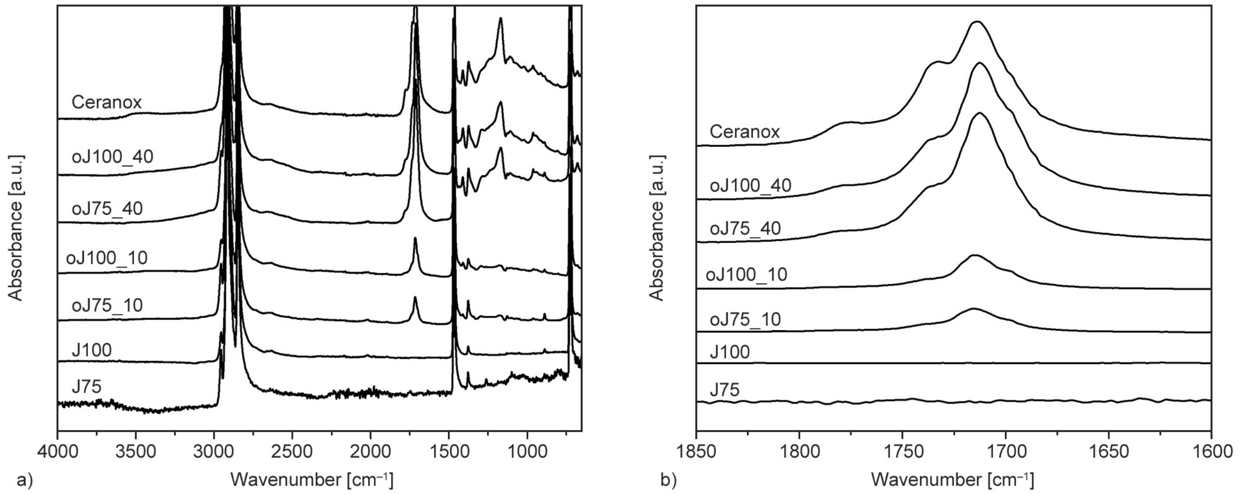

Figure 2. FTIR spectra of all waxes: a) the entire range and b) the carbonyl range.

smaller J75 wax molecule. An increase in the relative intensities of the chain end carbon signals compared to the backbone carbon signals was also observed as oxidation increased, indicating a possible decrease in molecular size or relative decrease in methylene signals due to the evolution of oxidative species as oxidation progressed. The downfield chemical shift region provided information on the electronically 'de-shielded' carbons of groups such as carbonyls (170–215 ppm) and alkenes (100–170 ppm) [19]. In these figures, clear evidence of carbonyl functional groups contributed by aldehydes and/or ketones (211 ppm) and carboxylic acids (176 ppm) was seen [20]. Initially, sample J75 showed a carbon spectrum resembling that of a linear hydrocarbon. Sample J100 also showed a similar spectrum except for an additional alkene signal. This indicated some unsaturation prior to ozone treatment, which was a significant finding as unsaturated carbons have increased reactivity and could be a reason for the slightly higher number of carbonyls in the oxidized J100 samples. Progress of the oxidation process was followed by the integration of the signal intensities of these carbons. Samples oJ75_10 and oJ100_10 which were subjected to lower amounts of ozone, showed some carbonyl and alkene formation. With higher ozone concentrations the signal intensity of aldehydes/ketones and carboxylic acids increased. This was a clear indication of further oxidation. Additionally, new peaks started developing in the aliphatic regions at 43, 34, 25, and 24 ppm, which were due to carbons in α and β positions to a specific carbonyl functional group. These carbons, together with their associated carbonyl groups, are shown in Table 4. It was difficult to assign these carbons to their respective groups in the aldehyde/ketone region as some overlap of signals

Table 3. ^{13}C-NMR integrals of the saturated hydrocarbon region.

	Saturated hydrocarbon integrals				
Carbon assignment	**Backbone**	**1s**	**2s**	**3s**	**4s**
Chemical shift [ppm]	**30**	**14.2**	**22.9**	**32.2**	**29.6**
J75	100	10.6	10.0	9.0	8.4
oJ75_10	100	10.9	10.4	8.9	9.0
oJ75_40	100	12.6	12.0	9.5	9.7
J100	100	5.7	5.5	5.2	4.8
oJ100_10	100	6.0	5.9	5.1	5.5
oJ100_40	100	6.5	6.3	5.6	7.1

Table 4. ^{13}C-NMR integrals of the carbonyl and alkene regions.

Carbon assignment	Carbonyl	α	β	Carbonyl	α	β	RC=CR
Chemical shift [ppm]	**211**	**43**	**24**	**176**	**34**	**25**	**121**
J75	–	–	–	–	–	–	
oJ75_10	0.2	0.4	0.4	0.2	0.2	0.2	0.2
oJ75_40	1.0	2.5	2.2	1.1	1.1	1.1	0.3
J100	–	–	–	–	–	–	0.1
oJ100_10	0.3	0.8	0.7	0.4	0.4	0.4	0.1
oJ100_40	1.0	3.3	3.4	2.0	2.0	2.0	0.3

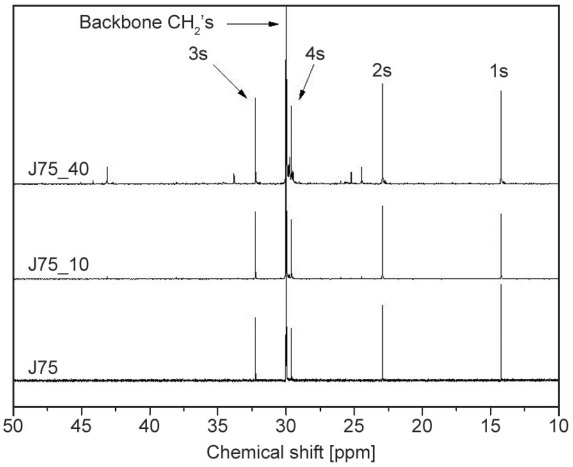

Figure 3. ^{13}C-NMR spectra of upfield chemical shift region for J75 samples.

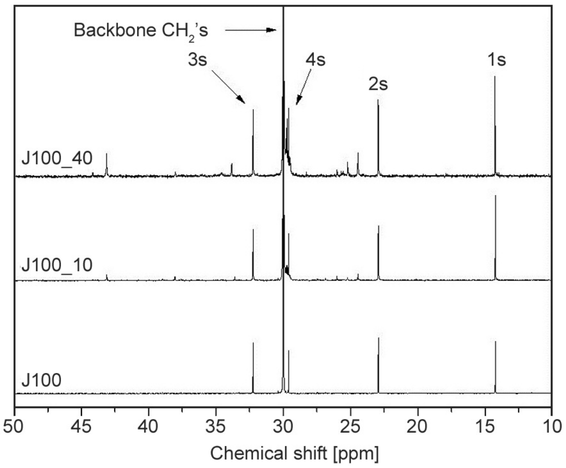

Figure 4. ^{13}C-NMR spectra of upfield chemical shift region for J100 samples.

occurred. There was, however, a definite twofold or threefold increase in intensity of these α and β carbons when compared to their respective carbonyl carbons. Further investigation into the direct quantification of aldehydes and ketones could be of great value, it was however seen as beyond the scope of this study. On the other hand, a clear ratio of 1:1:1 was observed for the carbonyl:α:β carbons of the carboxylic acid functional groups. This was in good agreement since carboxylic acid carbonyl moieties have only one α and β carbon associated with it. Unsaturation, however, remained relatively constant when compared to carbonyl formation.

4.1.3. Thermal behaviour

From differential scanning calorimetry (DSC) experiments, a total decrease in crystallinity was seen for both sample sets as oxidation increased. The total crystallinities for both sample sets decreased uniformly from roughly 80% to around 50%, as illustrated in Table 5. Figure 5 shows the melting endotherms of the waxes as a function of oxidation. There was a more noticeable shift in the melting endotherm maxima from a higher to a lower temperature for the J100 sample set with the progression of oxidation. For the J75 sample set, endothermic melting peak temperatures were less affected by oxidation. However, in both the J75 and J100 sets, a significant broadening in thermograms was seen with an increasing degree of oxidation, indicating more heterogeneous crystalline morphologies compared to the unoxidized, nonpolar neat wax counterparts. Both samples showed a characteristic FT wax multimodal melting peak distribution [21]. Multiple factors could affect the crystallinity of the samples. In the case of linear polyethylene molecules, the degree of crystallinity is influenced by the ability of the individual chains to come into close proximity and pack into dense crystallites, hence crystalline packing [22]. For linear hydrocarbons, this means that the degree of linearity should be high and that the degree of branching and presence of any other chemical pendant groups should be low. It was, therefore, expected that an increase in chain alterations would result in a decrease in chain uniformity, limiting the dense chain packing upon crystallization, which in turn would lead to a decrease in the degree of crystallinity. As seen from the preceding NMR results, there was a clear increase in oxygenate moieties together with an increase in chain end intensities. These newly functionalized moieties most likely behaved as crystallinity disrupters and led to other less crystalline domains, and hence the broadening of the thermal transitions seen by DSC.

These results were further accentuated by the crystallization data. In Table 6, the onset of crystallization, exotherm maxima, and crystallization enthalpy was seen to decrease with increasing oxidation levels

Table 5. DSC melting data of all wax samples.

Sample	Onset of melting [°C]	Endotherm maxima [°C]	Melt enthalpy [J/g]	Crystallinity[1] [%]
J75	47	73.4	238.1	81.2
oJ75_10	43	74.0	224.3	76.6
oJ75_40	31	69.0	152.7	52.1
J100	52	94; 110	236.2	80.6
oJ100_10	47	87; 105	216.3	73.8
oJ100_40	35	79; 98	151.6	51.7

[1] The standard heat of fusion for 100% crystalline PE of 293 J/g was used.

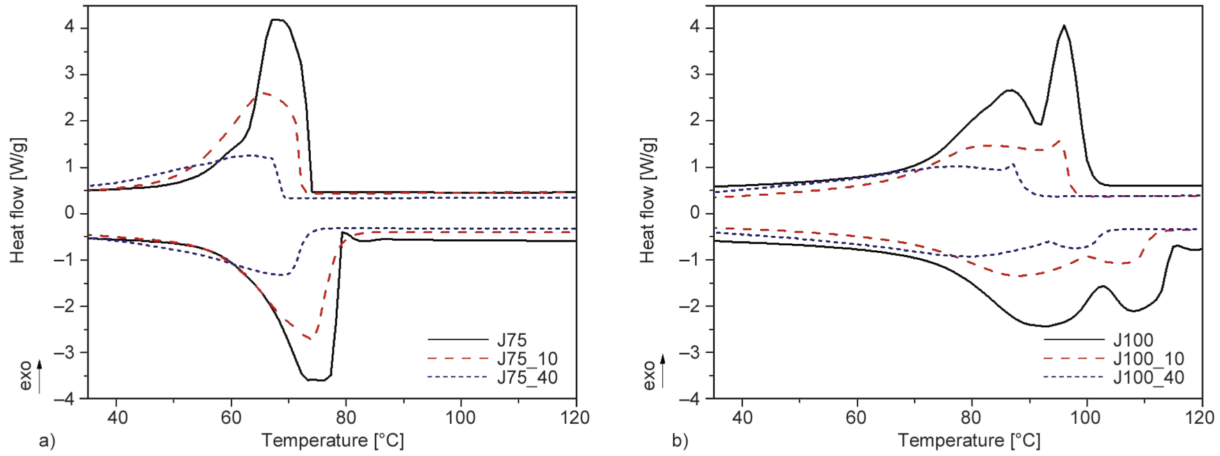

Figure 5. DSC thermograms of all wax samples: a) J75 series and b) J100 series.

Table 6. DSC crystallization data of all wax samples.

Sample	Onset of crystallization [°C]	Exotherm maxima [°C]	Crystallization enthalpy [J/g]
J75	74	68	226
oJ75_10	72	66	200
oJ75_40	69	62	133
J100	103	96; 86	231
oJ100_10	98	95; 83	199
oJ100_40	91	87; 77	123

for both sample sets. Figure 5 also shows a broadening of the crystallization exotherms. This was a clear indication of the crystallization behaviour being disrupted by the presence of oxygenate moieties along the hydrocarbon backbone.

4.1.4. Molecular weight analyses

To investigate if molecular size was affected by the oxidation process, high temperature size exclusion chromatography (HT-SEC) was carried out on the waxes. Polyethylene standards of known molecular weight (MW) were used as calibration for the calculation of the molecular weights of the samples. Table 7 illustrates that sample J75 had a smaller number-average molecular weight (M_n) of 525 g/mol compared to sample J100, with an M_n of 969 g/mol. As ozonolysis progressed, the general unimodal shape of the molecular weight distribution was maintained; however, the molecular weight distribution for both sample sets broadened. In Figure 6 it can be observed that sample oJ75_40 showed increased detector responses on both sides of the bulk elution peak at 25.5 ml compared to the neat J75 sample. This implies a simultaneous increase and decrease in H_v. The reason for a decrease in MW was due to the J75 molecules breaking up into smaller molecules during ozonolysis, similar to a chain scission effect. The increase in MW, which showed an increased elution peak between 24 and 25 ml, could be due to an association interaction between newly formed species or the effect of oxygenated moieties on the hydrodynamic volume of a sample relative to the nonpolar standards [23].

Table 7. HT-SEC results of all wax samples.

Sample	M_p [g/mol]	M_n [g/mol]	M_w [g/mol]	Đ
J75	515	525	564	1.1
oJ75_10	520	518	568	1.1
oJ75_40	510	489	617	1.2
J100	880	969	1142	1.2
oJ100_10	821	843	1057	1.3
oJ100_40	831	694	1012	1.5

M_p: Peak molecular weight.
M_n: Number-average molecular weight
M_w: Weight-average molecular weight

The molecular weight distribution increased for sample oJ100_40 but skewed only to the higher elution volume region. These large differences at higher volumes were most probably due to chain scission because of oxidation. These results show a similar trend as seen from the DSC thermograms. The decrease in crystallinity seen in Table 5 is accompanied by an increase in molecular weight dispersity seen in Table 7. This effect is more pronounced in the J100 sample set than in the J75 sample set. Both samples with the highest ozone exposure had decreased crystallinities of about 50%. The dispersity of oJ100_40, however, was much larger at 1.5 compared to the oJ75_40 sample, which had a dispersity of only 1.2. This shows that by only changing the degree of dispersity slightly for the smaller J75 sample set had a much greater effect on the crystallinity thereof. As mentioned in the DSC section, chain uniformity is an important parameter for linear hydrocarbon crystallinity. An effective way to evaluate this parameter is by measuring the ethylene sequence length of a sample. A liquid chromatography experiment was therefore

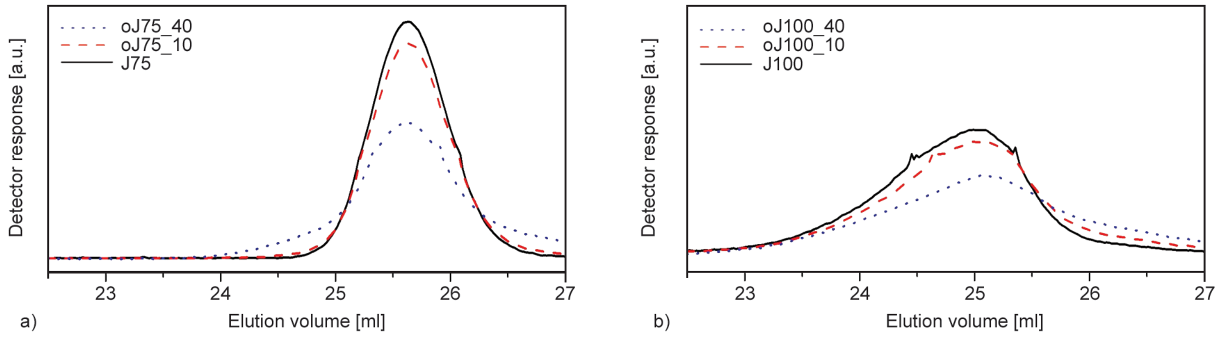

Figure 6. HT-SEC chromatograms of a) J75 and b) J100 waxes.

conducted to investigate the ethylene sequence lengths of the waxes to gain further insight into the oxidized wax compositions.

4.1.5. High temperature - solvent gradient interaction chromatography (HT-SGIC)

HT-SGIC was used to probe the nonpolar ethylene sequence lengths (ESL) of the waxes. This was achieved by fractionating wax samples on a nonpolar porous graphite column (stationary phase) combined with a controlled solvent gradient elution profile (mobile phase). By using a nonpolar stationary phase, the nonpolar ethylene sequences are adsorbed onto it by means of van der Waal's force interactions. Initially, the mobile phase was in isocratic mode, using decane as solvent. During isocratic mode, any weak adhering molecules, such as molecules with short ESLs, eluted with the decane solvent, whereas molecules with longer ESLs had higher affinity and adsorbed to the stationary phase. Gradual addition of a desorption promoting solvent, such as dichlorobenzene, to the mobile phase allowed for molecular species with stronger adsorption to the stationary phase (or longer ESLs) to desorb from the column and elute. Using a solvent gradient meant that the elution of molecular species could be controlled in order of increasing affinity for the column and hence separation according to ESL. In this experiment, all samples were doped with a standard linear C_{50} hydrocarbon oligomer marker to comparatively evaluate the chain length of the eluted material. When comparing Figures 7 and 8, a clear difference in elution profiles can be seen with the J75 sample set eluting much earlier than the J100 sample set. The bulk of the J75 samples also eluted before the C_{50} marker, whereas the peak of the J100 samples eluted around the same time as the marker. In addition, the J75 series showed narrower elution profiles compared to the J100 samples, correlating with the narrower, more homogeneous molecular weight distribution seen for the J75 series in HT-SEC. It can, therefore, be concluded that the J75 sample set consisted of short and narrow ESL distributions, whereas the J100 samples exhibited longer ethylene sequences and broad ESL distributions. These results compare well with the trends seen from the HT-SEC experiments, from which it was concluded that as the ethylene sequences were interrupted, they were broken down into shorter chains.

The effect of oxidation was seen in both sample sets, resulting in a decrease in the signal during isocratic conditions with increasing ozone exposure. Ndiripo and Pasch [24] have shown this to be a result of the difficulty in detecting multifunctional species within the evaporative light scattering detector (ELSD). In their study on oxidized and non-oxidized waxes, it was concluded that the decrease in detector signal was due to the fact that neat apolar waxes have different refractive indices than waxes with oxygenate functionalities. In both cases, the signal decreased throughout the entire elution profile range. From these results, it can, therefore, be concluded that the entire ESL range was disrupted by oxygenate functionality. Hence, the ozonolysis process had no major preference for affecting either the shorter or longer chain sequences within the waxes.

In addition, to reverse-phase SGIC, waxes were also fractionated using a polar silica column together with a nonpolar mobile phase. During isocratic mode, it allowed all non-retained nonpolar wax molecules to elute. Thereafter, the polarity of the mobile phase was increased by the systematic addition of a

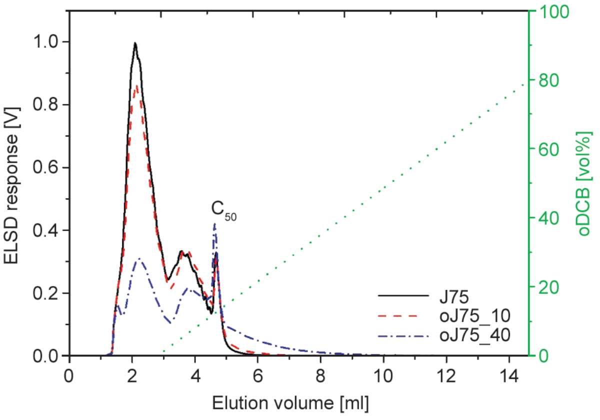

Figure 7. Reverse-phase HT-SGIC elution profiles for the J75 sample set.

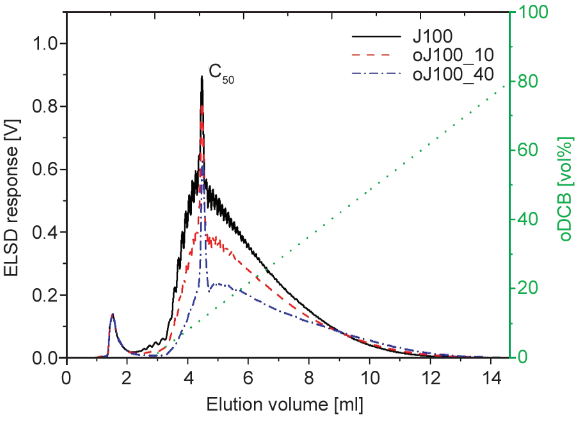

Figure 8. Reverse-phase HT-SGIC elution profiles for the J100 sample set.

desorption promoting polar solvent (1-hexanol). This resulted in the desorption of slightly retained (slightly oxidized) material. By further increasing the mobile phase polarity, the strongly retained (highly oxidized) material could be eluted [24]. The polarity of a wax is governed by the concentration, distribution, and type of oxygenates present along the molecular chain. In each sample set, the neat samples eluted entirely during the isocratic mode at around 3 mL (Figures 9 and 10). This nonpolar peak broadened as oxidation increased, and the broadening was more pronounced for the J100 sample set. This might be due to the larger J100 molecules, which consist of a longer nonpolar chain segment, resulting in a relatively higher nonpolar contribution to the overall polarity of the sample. This is also in alignment with the greater SEC dispersity observed for the heavier J100 set. As oxidation increased, the nonpolar peak intensity decreased as a new peak started appearing at around 9 ml. These emerging peaks at later elution volumes were due to chains with higher polarity. For eluting the highly oxidized fractions, the volume of 1-hexanol was increased considerably. Samples oJ75_40 and oJ100_40 showed a highly oxidized sample peak at around 11.5 ml.

The preceding data shows that two linear hydrocarbon FT waxes of different molecular weights were successfully oxidized to varying degrees. In both sample sets, two degrees of oxidation were achieved by varying the amount of ozone gas introduced to each sample. Initially, the level of oxidation was tracked using an off-line ATR-FTIR analysis technique where the carbonyl region was measured relative to the hydrocarbon methylene stretching bands. The types of oxygenates were probed using quantitative ^{13}C-NMR. DSC analysis showed that the inclusion of these oxygenates interrupted the crystallinity and melting behaviour of the samples. HT-SEC and HT-SGIC showed complimentary results where after it could be concluded that the samples were broken down into shorter chains as the ESL was influenced. The subsequent section discusses the approach to evaluate the waxes in PVC blends during extrusion and fusion experiments.

4.2. Extrusion and fusion of PVC blends

SEM-EDS images in Figure 11 show all the screw freezing experiments for both binary (PVC/wax) and ternary (PVC/wax/CaSt) PVC blends. Sample oJ75_10 showed a completely fused PVC matrix for the binary blend (Figure 11a) but not for the ternary blend (Figure 11e), where some wax inclusion could still be observed in the ternary blend. Sample oJ75_40, however, showed complete fusion in both the binary and the ternary blend.

From previous screw freezing attempts, it was observed that high melting waxes (melting above the T_g of PVC), such as neat J100, did not fuse at these extruder conditions and needed either higher experimental temperatures or lower lubricant concentrations. Figure 12, however, shows that the neat J75 sample completely fused during extrusion. Experiments that followed showed that polar waxes, also consisting of peak melting points above the T_g of PVC, did in fact fuse at these extruder conditions. It was therefore concluded that the effect of polarity played a big role in fusion behaviour. Interestingly, in this sample set of oxidized FT waxes, sample oJ100_10 also showed insufficient fusion for both the binary and ternary samples (Figures 11c and 11g). This could be seen by the disruption of the chloride signal uniformity. Sample oJ100_40 with a higher

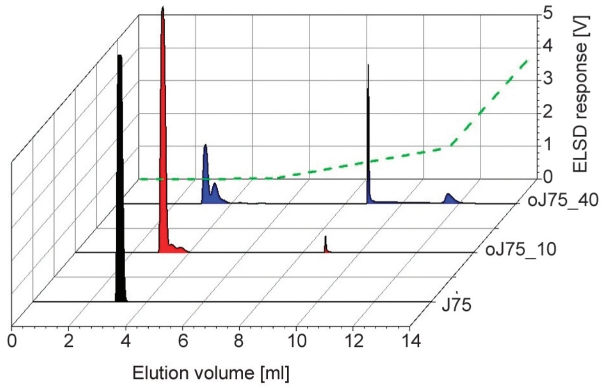

Figure 9. Normal-phase HT-SGIC elution profiles of the J75 sample set. Relative 1-hexanol flow rate = green dashed line (– – –).

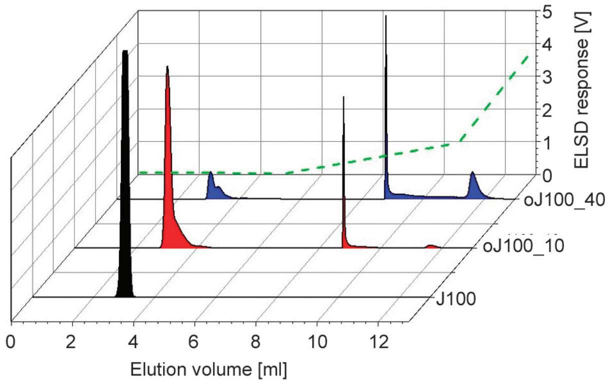

Figure 10. Normal-phase HT-SGIC elution profiles of the J100 sample set. Relative 1-hexanol flow rate profile = green dashed line (– – –).

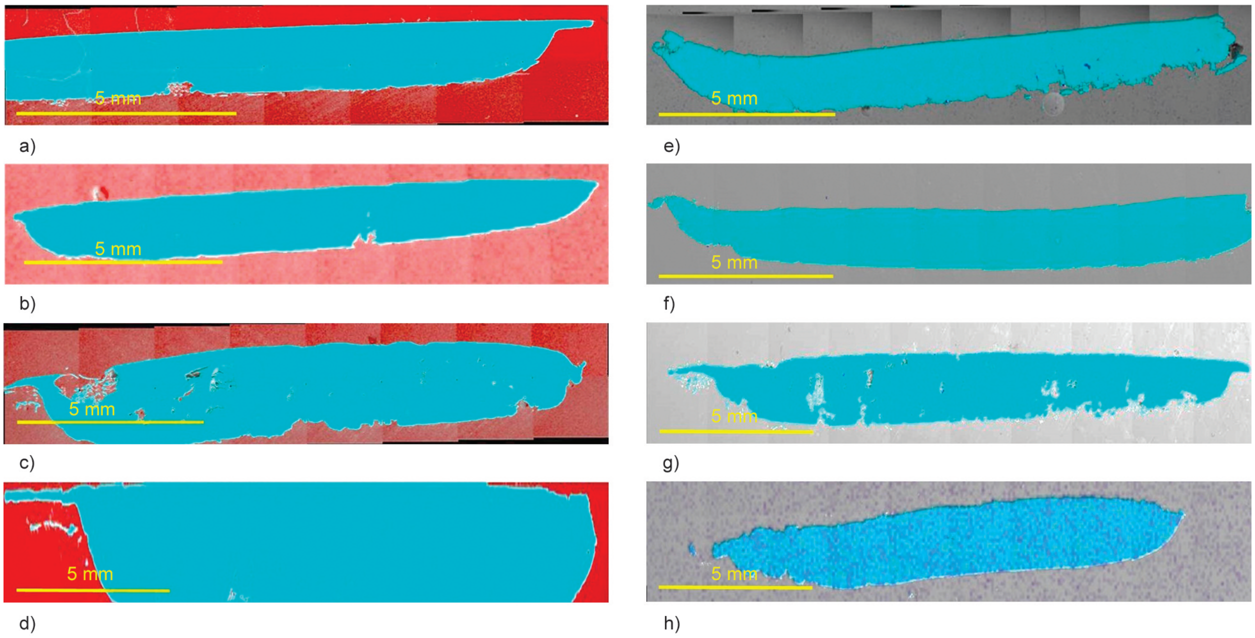

Figure 11. SEM-EDS images of binary blends a) oJ75_10; b) oJ75_40; c) oJ100_10 and d) oJ100_40 and ternary blends e) oJ75_10; f) oJ75_40; g) oJ100_10 and h) oJ100_40 after screw freezing. Electron image = grey; Chloride = blue; Carbon = red. Scale bar = 5 mm.

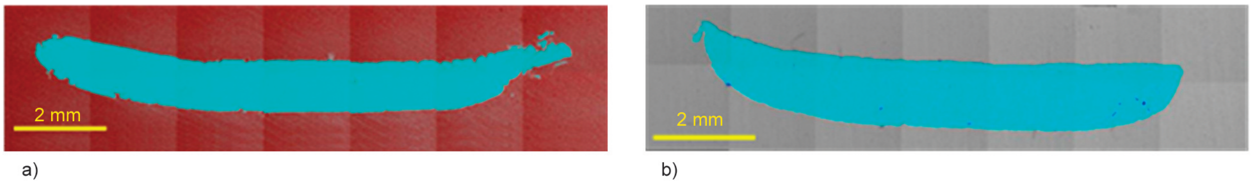

Figure 12. SEM-EDS images of neat nonpolar J75 a) binary and b) ternary blends after screw freezing. (neat J100 sample could not be micrographed). (Color codes similar to Figure 11.) Scale bar = 2 mm.

degree of oxidation showed complete fusion and did, however, also have a decreased melting temperature due to the oxidation process (Figure 5b). The effect on fusion could, therefore, not only be ascribed to an increased oxidation level and hence polarity but an additional effect of decreased melting point and differences in molecular chain mobility should also be considered. It was however clear that for complete fusion to take place, the wax has to migrate out of the PVC matrix. It should be noted that the purple colour seen in Figure 11h was contributed by the instrumentation background signal and not due to CaSt, as the signals were observed in the sample stage surrounding the PVC as well.

Performing fusion studies on the Brabender extruder could not provide much information on fusion times and efficiency. To further investigate the effect on fusion parameters, it was decided to do a series of fusion studies on these PVC blends using a more commercially relevant torque rheometry method.

During the screw freezing experiments, it was concluded that the waxes plated out (migrated to extrudate surface) due to their absence in the SEM-EDS micrographs (Figure 11). To further investigate if these synthesized waxes had any effect on the fusion behaviour of Sn-stabilized uPVC formulations, a series of fusion studies were proposed using a torque rheometer. Commercially relevant lubricant concentrations were used to formulate PVC blends that are comparable to that of approved industry formulations. The formulations that were tested are listed in Table 1. Apart from the full ternary formulation, containing both internal and external lubricants, binary blends were also analysed to investigate the fusion behaviour in the absence of the calcium stearate component.

Figure 13 shows the fusion curves of the ternary blends. Figure 13a illustrates that the unoxidized J75 sample did not fuse at 185 °C. It also shows that by slightly increasing the level of oxidation, fusion was promoted with an increase in torque as fusion time decreased. This effect, however, might not solely be due to increased polarity, but as was observed from the preceding characterization sections, oxidation affected the wax properties in various ways. The

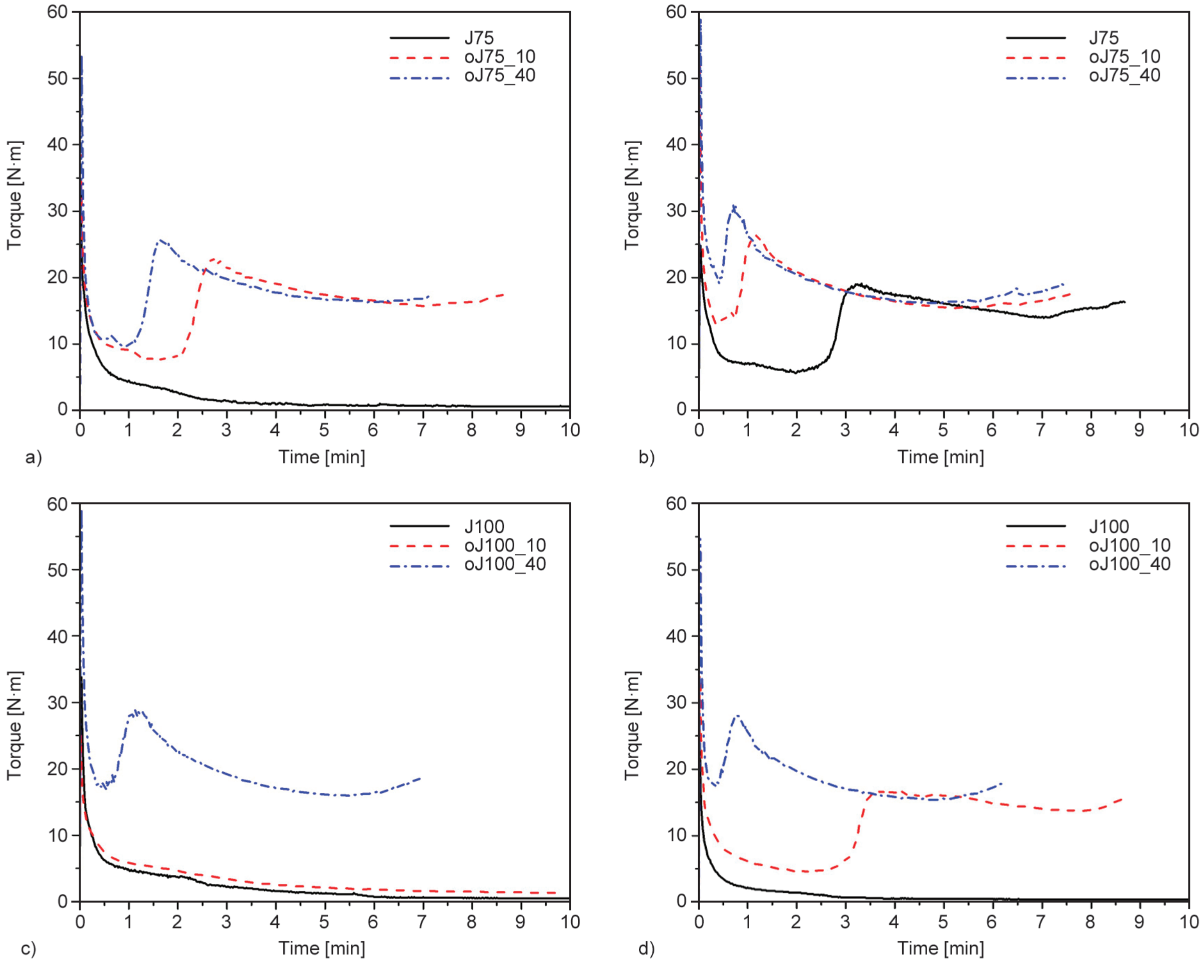

Figure 13. Fusion curves of ternary blends of the J75 series at a) 185 °C and b) 190 °C and the J100 series at c) 185 °C and d) 190 °C.

melting temperature and molecular size decreased with increased oxidation, both of which could lead to earlier fusion. The overall effect can, therefore, not only be ascribed to an increase in polarity but a combination of effects should be considered. Figure 13b shows that by increasing the temperature, fusion was promoted for the unoxidized J75 sample. Additionally, for the oxidized samples, differences in fusion times were less noticeable with an increase in temperature due to the increase in thermal energy overcoming the smaller morphological differences and intermolecular forces at play. As observed in Figure 13c, no fusion was observed for both the unoxidized J100 and oxidized oJ100_10 samples at the lower experimental temperature of 185 °C, despite oJ100_10 having comparable oxidation levels to oJ75_10. This could, therefore, be due to the molecular size or melting temperature differences between the two samples. As the temperature was increased to 190 °C in Figure 13d, both oxidized oJ100_10 and oJ100_40 resulted in fusion. The neat, unoxidized, nonpolar J100 wax formulation needed even higher thermal energy (above 190 °C) to promote fusion. This clearly implies that by slightly increasing the level of oxidation in the wax, practical fusion times can be achieved compared to their difficult-to-fuse nonpolar counterpart lubricant formulations. When comparing the two sample sets, the J75 series were more versatile with respect to changes in experimental conditions. It indicates that the degree of oxidation influenced the fusion behaviour and that the effect was more accentuated for the smaller J75 wax molecules since the oJ75_10 sample fused at 185 °C, whereas the oJ100_10 did not fuse. Furthermore, the effect of oxidation on the other morphological properties of the lubricants, such as thermal behaviour, molecular chain length, melt viscosity, and molecular chain mobility, also plays an important role in controlling the fusion behaviour of a PVC formulation. When comparing all the highly oxidized samples (40% oxidation), all showed similar, rapid fusion with fusion times of about 1 min and fusion torque values of about 30 N·m. The lower oxidized samples (10% oxidation) however showed more varying fusion behaviour. High friction leads to rapid fusion due to decreased lubrication efficiency. This suggests that there exists an oxidation limit where the wax loses its lubricating properties and migrates out of the PVC matrix more rapidly. There should, therefore, exist an inflection point where the level of oxidation becomes the dominating factor when compared to other wax properties, such as melting point, molecular size, and molecular chain mobility (melt viscosity). Also, oJ100_10 showed a similar fusion profile to that of unoxidized J75 at 190 °C, which highlights the possibility that similar fusion profiles can be achieved by simply modifying the degree of oxidation of a hydrocarbon wax. Stable times (time between fusion peak to onset of degradation) of the formulations remained fairly unaffected with an increase in oxidation level, which is an interesting finding as this shows shorter fusion times with minimal changes in formulation stability. Stable times decreased marginally with an increase in experimental temperature. The fusion behaviour of binary PVC systems containing only PVC and wax was also investigated (Figure 14). These samples were expected to show a delay in fusion with the absence of an internal fusion promoter, as per conventional lubricant classifications [25]. This was, however, not the case, as all the samples fused rapidly in under 2 min. The cause for this behaviour could be that too little wax lubricant was present in the formulation, which resulted in the rapid fusion thereof. Although the wax concentration was constant for binary and ternary systems, excluding the calcium stearate in the binary blends lowered the total lubricant concentration, which led to increased friction and, therefore, earlier fusion. This suggests that if the effect of a binary system, using modified wax as a multifunctional lubricant, is to be investigated, careful considerations are needed in adjusting lubricant concentrations.

Comparing these findings to the SEM-EDS micrographs during the screw freezing experiments provided plenty of information to try and explain the mechanism at hand. It should however be remembered that

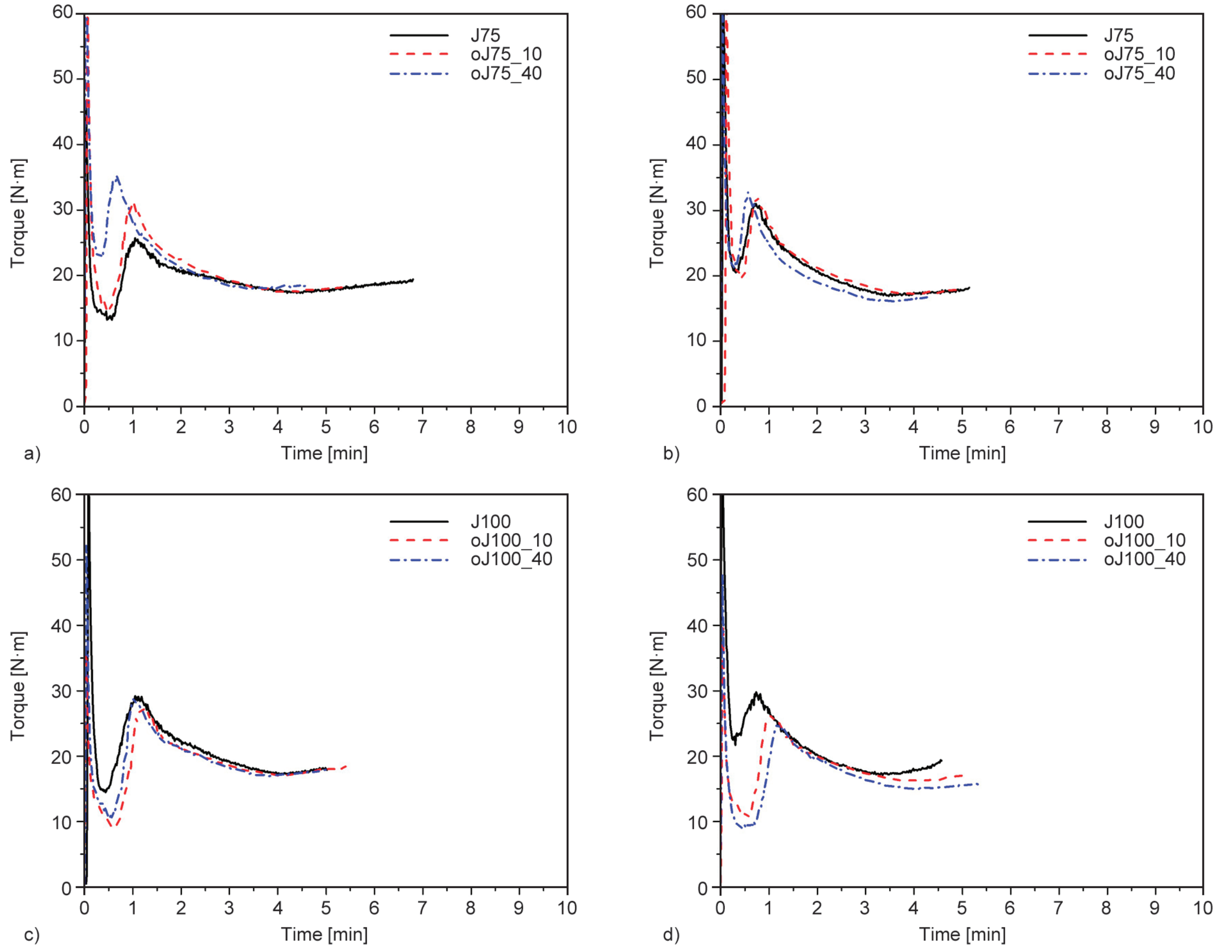

Figure 14. Fusion curves of binary blends of the J75 series at a) 185 °C and b) 190 °C and the J100 series at c) 185 °C and d) 190 °C.

during screw freezing, the temperature was set to 190 °C and that higher wax concentrations were used for the formulations. The neat unoxidized J75 screw freezing micrograph in Figure 12 showed complete fusion in both the binary and ternary blends. These two results correlated well with the torque rheometer fusion studies, as complete fusion was seen for the neat J75 sample, and no fusion was observed for the J100 sample. From this data, it can be concluded that due to the absence of wax in the micrographs, for complete fusion to have occurred, all the wax must have migrated outwards toward the instrument sidewalls. The J100 formulation, however, remained in powder form and did not fuse, which means that these larger wax molecules took too long to migrate out to the sidewalls. This could be overcome by the addition of more thermal energy, which would result in increased molecular motion of the wax molecules and, therefore, promote fusion. In Figure 11, all the samples, except for oJ100_10, showed complete fusion, emphasizing that for complete fusion to take place, all the lubricant needs to be expelled from the PVC matrix. For the explanation of the fusion trends that were observed for increasing wax oxidation levels, the mechanism of surfactants and slip agents proposed by Rabinovitch can be used. In this mechanism, CaSt acts as a surfactant, and wax acts as a slip agent. A nonpolar wax would, therefore, have the lowest degree of association with the CaSt/PVC system and therefore delay the fusion to a greater extent. As oxidation is increased, the degree of chemical association between the CaSt and the wax is also increased. This was also observed in a preceding investigation [17]. The CaSt would then also show greater association towards the wax and therefore migrate away from the PVC with the lubricant. Lubricant migration from the PVC particles causes greater internal friction between the particles, which results in earlier fusion.

5. Conclusions

Two sets of oxidized FT waxes were successfully synthesized following a controlled ozonolysis procedure. This resulted in two sets of well-defined oxidized waxes with varying degrees of oxidation, which were fully characterized using various analytical techniques. Some key correlations that were established are as follows: FTIR results correlated well with NMR, where an increase in oxygenates was observed with an increase in the degree of ozonolysis. HT-SEC results confirmed that molecular chains were shortened and showed a broadened molecular weight distribution with increased ozone exposure. This result was well aligned with DSC thermograms that showed a decrease in overall crystallinity as ozonolysis progressed. HT-SGIC illustrated that functionalization of the wax molecules occurred across the entire molecular distribution.

Screw freezing experiments revealed that all the samples fused completely except for the J100 and slightly oxidised oJ100_10 samples. However, the oJ100_40 sample did fuse, which showed that oxidation did promote fusion. These findings accentuate that on-purpose oxidation of waxes can be a useful protocol to follow and allows for alteration of parameters such as polarity, molecular weight, melting point, and viscosity that, in turn, has a significant effect on the fusion behaviour of the resultant PVC blends.

Fusion studies indicated that fusion could be promoted with an increasing degree of oxidation of external wax lubricant. By combining the results from the screw freezing and fusion experiments, it was possible to expand on the current model proposed by Rabinovitch. As the formulation is introduced into the extruder, the lubricant system has to migrate away from the PVC to the extruder sidewalls to promote fusion of the PVC matrix. Rapid migration therefore leads to shorter fusion times. In the case of the nonpolar waxes at low temperatures, this does not occur easily. When the molecules are oxidized or the mobility is increased with increased temperature, the lubricant system migrates from the PVC matrix sufficiently. The lubricant system, which contains the wax and CaSt has to migrate towards the metal interface. The migration of the lubricant system is governed by the association interaction between the wax and CaSt together with the combined mobility of the associated molecules. The composition of this combination therefore governs the fusion rate. By increasing the wax polarity and therefore the wax-CaSt interaction, or by increasing the mobility through temperature, the rate of migration can be manipulated. The findings of this study show that it might be useful to investigate the use of oxidized waxes as multifunctional lubricants during PVC processing.

Acknowledgements

The authors would like to thank the Central Analytical Facilities (CAF) at the University of Stellenbosch for their assistance with the microscopy and spectroscopy work.

References

[1] Demirci A., Teke I., Goger A., Canbaz E., Vlachopoulos J.: Gelation of poly(vinyl chloride) inside a single screw extruder and its effect on product properties. Journal of Vinyl and Additive Technology, **25**, E174–E180 (2019). https://doi.org/10.1002/vnl.21676

[2] Mohamed N. A.: Antimicrobial itaconimido aromatic hydrazide derivatives for inhibition of the thermal degradation of rigid PVC. Polymer Bulletin, **76**, 2341–2365 (2019). https://doi.org/10.1007/s00289-018-2486-8

[3] Moore S.: Global trends in PVC resin applications and additives usage. in 'PVC AUS 2018: Shaping the Future. Sydney, Australia' Townsend Solutions, Houston, 1–33 (2018).

[4] Gilbert M., Patrick S.: Poly(vinyl chloride). in 'Brydson's plastics materials' (ed.: Gilbert M.) Elsevier, Amsterdam, 329–388 (2017). https://doi.org/10.1016/B978-0-323-35824-8.00013-X

[5] Moghri M., Garmabi H., Akbarian M.: Effects of additives on fusion parameters of rigid PVC formulations. Journal of Vinyl and Additive Technology, **14**, 73–78 (2008). https://doi.org/10.1002/vnl.20148

[6] Schiller M.: PVC additives. Hanser, Munich (2015).

[7] Kendall M. J., Siviour C. R.: Strain rate dependence in plasticized and un-plasticized PVC. EPJ Web of Conferences, **26**, 02009 (2012). https://doi.org/10.1051/epjconf/20122602009

[8] Papakonstantinou V., Papaspyrides C. D.: Plasticizer migration from plasticized into unplasticized poly(vinyl chloride). Journal of Vinyl Technology, **16**, 192–196 (1994). https://doi.org/10.1002/vnl.730160404

[9] Shimpi N. G., Verma J., Mishra S.: Preparation, characterization and properties of poly(vinyl chloride)/$CaSO_4$ nanocomposites. Plastics Technology and Engineering, **48**, 997–1001 (2009). https://doi.org/10.1080/03602550902824689

[10] Mosoabisane M. F. T., van Sittert C. G. C. E., Luyt A. S.: Molecular dynamics on blend miscibility of LLDPE and soft wax: An atomistic simulation and thermodynamic approach. Express Polymer Letters, **17**, 546–562 (2023). https://doi.org/10.3144/expresspolymlett.2023.40

[11] Moghri M., Garmabi H., Akbarian M.: Effect of processing parameters on fusion and mechanical properties of a twin-screw extruded rigid PVC pipe. Journal of Vinyl and Additive Technology, **9**, 81–89 (2006). https://doi.org/10.1002/vnl.10067

[12] Rabinovitch E. B., Lacatus E., Summers J. W.: The lubrication mechanism of calcium stearate/paraffin wax systems in PVC compounds. Journal of Vinyl Technology, **6**, 98–103 (1984). https://doi.org/10.1002/vnl.730060303

[13] Mondragón M., Flores A. C.: The effect of combining lubricants on fusion behavior of rigid PVC. Journal of Vinyl Technology, **15**, 46–50 (1993). https://doi.org/10.1002/vnl.730150203

[14] Rabinovitch E. B., Isner J. D., Sidor J. A., Weidl D. J.: Effect of extrusion conditions on rigid PVC foam. Journal of Vinyl and Additive Technology, **3**, 210–215 (1997). https://doi.org/10.1002/vnl.10193

[15] Summers J. W.: Lubrication mechanism of poly(vinyl chloride) compounds: Changes upon PVC fusion (gelation). Journal of Vinyl and Additive Technology, **11**, 57–62 (2005). https://doi.org/10.1002/vnl.20037

[16] Treffler B.: Impact of lubricants on processing behaviour of U-PVC. Plastics, Rubber and Composites, **34**, 143–147 (2005). https://doi.org/10.1179/174328905X55506

[17] Barnard J. L., Robertson D. D., van Reenen A. J.: Tracking lubricants during single screw extrusion of uPVC. Polymer Testing, **87**, 106523 (2020). https://doi.org/10.1016/j.polymertesting.2020.106523

[18] Motaung T. E., Luyt A. S.: Effect of maleic anhydride grafting and the presence of oxidized wax on the thermal and mechanical behaviour of LDPE/silica nanocomposites. Materials Science and Engineering, **527**, 761–768 (2010). https://doi.org/10.1016/j.msea.2009.08.065

[19] Diehl B.: NMR applications for polymer characterization. in 'NMR spectroscopy in pharmaceutical analysis' (Holzgrabe U., Wawer I., Diehl B.) Elsevier, Amsterdam, 157–180 (2011). https://doi.org/10.1016/B978-0-444-53173-5.00007-X

[20] Cistola D. P., Small D. M., Hamilton J. A.: Carbon 13 NMR studies of saturated fatty acids bound to bovine serum albumin. I. The filling of individual fatty acid binding sites. Journal of Biological Chemistry, **262**, 10971–10979 (1987). https://doi.org/10.1016/S0021-9258(18)60913-5

[21] Novák I., Krupa I., Luyt A. S.: Modification of a Fischer-Tropsch wax by grafting with maleic anhydride. Journal of Applied Polymer Science, **93**, 662–668 (2004). https://doi.org/10.1002/app.20513

[22] Méndez C. I., Ancheyta J.: Kinetic models for Fischer-Tropsch synthesis for the production of clean fuels. Catalysis Today, **353**, 3–16 (2020). https://doi.org/10.1016/j.cattod.2020.02.012

[23] Ndiripo A., Pasch H.: A multidimensional fractionation protocol for the oligomer analysis of oxidized waxes. Analytica Chimica Acta, **1027**, 137–148 (2018). https://doi.org/10.1016/j.aca.2018.03.007

[24] Ndiripo A., Pasch H.: Comprehensive analysis of oxidized waxes by solvent and thermal gradient interaction chromatography and two-dimensional liquid chromatography. Analytical Chemistry, **90**, 7626–7634 (2018). https://doi.org/10.1021/acs.analchem.8b01480

[25] Pedersen T. C.: Process and material considerations in the industrial application of lubricants in rigid PVC extrusion. Journal of Vinyl Technology, **6**, 104–109 (1984). https://doi.org/10.1002/vnl.730060304